

Spin Diffusion in the $S = 1/2$ Quasi One-Dimensional Antiferromagnet α -VO(PO₃)₂ via ³¹P NMR

Jun KIKUCHI*, Naohiko KURATA, Kiyochiro MOTOYA,
Touru YAMAUCHI¹ and Yutaka UEDA¹

*Department of Physics, Faculty of Science and Technology, Science University of Tokyo,
2641 Yamazaki, Noda, Chiba 278-8510*

¹*Institute for Solid State Physics, University of Tokyo, 5-1-5 Kashiwanoha, Kashiwa, Chiba 277-8581*

(Received February 15, 2001)

Low-frequency spin dynamics in the $S = 1/2$ antiferromagnetic spin-chain compound α -VO(PO₃)₂ has been studied by means of ³¹P NMR. The nuclear spin-lattice relaxation rate $1/T_1$ at the P site exhibits $H^{-1/2}$ dependence on the applied magnetic field (H) at temperatures (T) well above the intrachain coupling strength $J/k_B = 3.50$ K indicating one-dimensional diffusive spin dynamics. The diffusive contribution to $1/T_1$ decreases on cooling as electronic spins acquire short-range antiferromagnetic correlations within the chain, and vanishes almost entirely around $T \approx J/k_B$. This is accompanied by an apparent increase of the spin-diffusion constant from the value expected in the classical limit. On the other hand, the field-independent part of $1/T_1$ increases with decreasing temperature, which may be a precursor for the true long-range antiferromagnetic ordering found below $T_N = 1.93 \pm 0.01$ K.

KEYWORDS: α -VO(PO₃)₂, NMR, antiferromagnetic spin chain, nuclear spin relaxation, spin diffusion

§1. Introduction

There has been a continued interest in the dynamics of low-dimensional quantum antiferromagnets at finite temperatures. One of the issues which has attracted renewed attention is a problem of spin diffusion in the one-dimensional (1D) Heisenberg spin chain. It is argued from phenomenology that at high enough temperatures and at long times, the spin autocorrelation function of the 1D Heisenberg spin chain has a diffusive form

$$\langle S_i(t)S_i(0) \rangle \propto t^{-1/2}, \quad (1.1)$$

leading to divergence of the spectral density at low frequencies as $\omega^{-1/2}$. However, because the diffusive form (1.1) is not derived from the microscopic Hamiltonian but is a consequence of the hydrodynamical assumption for the spin-spin correlation,¹⁾ the question on the existence of spin diffusion in 1D spin chains has been studied intensively from both theoretical and experimental viewpoints. One of the best studied theoretical models is the $S = 1/2$ XXZ chain represented by the Hamiltonian^{2,3,4,5,6,7)}

$$\mathcal{H} = J \sum_i (S_i^x S_{i+1}^x + S_i^y S_{i+1}^y + \Delta S_i^z S_{i+1}^z). \quad (1.2)$$

At the isotropic point ($\Delta = 1$) and at low enough temperatures ($T \ll J/k_B$), analytical expressions for the dynamical susceptibility $\chi(q, \omega)$ have been derived for $q \approx 0$ and π , and are shown to have no diffusive pole at low frequencies.²⁾ At modestly high, or much higher temperatures compared with the intrachain coupling strength J , the problem is still controversial. Although the absence

of diffusive excitations seems to be settled for the XXZ chain with planar anisotropy ($0 \leq \Delta < 1$), a definite answer for the absence (or presence) of spin diffusion at the isotropic point has not yet been given.

Diffusive behavior of the spin-spin correlation has been observed experimentally in several 1D spin chains via the $\omega^{-1/2}$ resonance-frequency dependence of the nuclear spin-lattice relaxation rate $1/T_1$ at elevated temperatures.^{8,9,10,11,12,13)} As to the $S = 1/2$ chain, an analysis of the ω dependence of $1/T_1$ at the Cu site in Sr₂CuO₃ based on the classical spin-diffusion theory gives an unusually high value of the spin diffusion constant compared with the classical value.¹⁴⁾ This suggests the absence of spin diffusion in the low-temperature limit in consistency with the field-theoretical²⁾ and perturbative³⁾ approaches. On the other hand, an evidence for diffusive spin transport is found from the proton NMR measurements in CuCl₂·2NC₅H₅ and Cu(C₆H₅COO)₂·3H₂O at temperatures well above the intrachain exchange interactions.¹¹⁾ Therefore, there seems to be a gap between the high- and low-temperature behavior of the spin transport in the $S = 1/2$ chains, necessitating further experiments on the dynamics, especially on the temperature-dependent properties.

Linear chains of a V⁴⁺ ion in the compound α -VO(PO₃)₂ may be a model system of an $S = 1/2$ Heisenberg spin chain. α -VO(PO₃)₂ belongs to the monoclinic space group $C2/c$ and has the room-temperature lattice parameters; $a = 15.140$ Å, $b = 4.195$ Å, $c = 9.573$ Å and $\beta = 120.54^\circ$.¹⁵⁾ In the α -VO(PO₃)₂ structure (Fig. 1), VO₅ pyramids are stacked along the b axis to make up a linear chain of V atoms with the nearest-neighbor V-V distance of 4.915 Å. The linear chains are well separated by distorted PO₄ tetrahedra in the a and c di-

* E-mail: kikuchi@ph.noda.sut.ac.jp

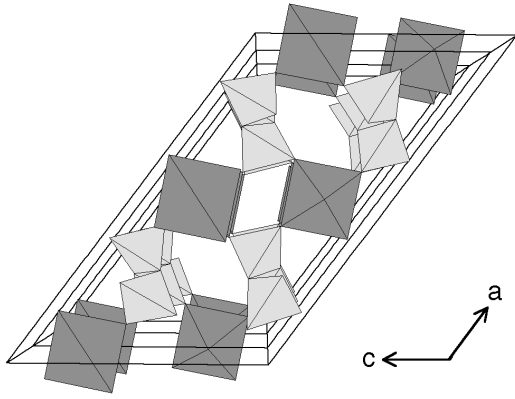


Fig. 1. Crystal structure of α -VO(PO₃)₂ viewed from the monoclinic b axis. The dark- and light-shaded polyhedra represent VO₅ pyramids and PO₄ tetrahedra, respectively.

rections, so that good one dimensionality in the b direction is expected. In this paper, we report on the experimental study of the low-frequency spin dynamics in α -VO(PO₃)₂ via ³¹P NMR. The relatively small intrachain coupling ($J/k_B = 3.50$ K estimated from the present susceptibility measurement) in α -VO(PO₃)₂ enables us an experimental access to a wide range of temperatures not only $T \sim J/k_B$ where short-range antiferromagnetic correlations are important, but also $T \gg J/k_B$ where electronic spins behave almost paramagnetically. Crossover of the dynamics between the two temperature regimes can also be elucidated by examining the temperature-dependent behavior of, for example, the nuclear spin-lattice relaxation rate. This type of the experiment cannot be done in the canonical $S = 1/2$ Heisenberg antiferromagnetic spin-chain compound Sr₂CuO₃ which has a huge intrachain exchange ($J/k_B = 2200$ K)¹⁶⁾ being suitable for the study of low-temperature dynamics, and will give complementary information for thorough understanding of low-energy spin excitations in the $S = 1/2$ Heisenberg spin chain.

§2. Experiments

Polycrystalline samples of α -VO(PO₃)₂ were prepared by a solid-state reaction method. Equimolar mixture of (VO)₂P₂O₇ and P₂O₅ was fired in an evacuated silica tube at 750 °C for 2 days and at 900 °C for 2 days with the intermediate grinding. (VO)₂P₂O₇ was prepared as described in ref. 17. The obtained samples were examined by the X-ray diffraction measurement and were confirmed to be a single phase. Magnetic susceptibility was measured using a SQUID magnetometer (Quantum Design MPMS-5s) at 0.1 T. NMR measurements were performed with a standard phase-coherent pulsed spectrometer. ³¹P NMR spectrum was taken by recording the spin-echo signal with a Box-car averager at a fixed frequency while sweeping the external magnetic field. The nuclear spin-lattice relaxation rate of ³¹P was measured by a saturation recovery method with a single saturation rf pulse. The measured nuclear-magnetization recoveries were single exponential as expected for nuclei with spin 1/2, so that the nuclear spin-lattice relaxation time T_1

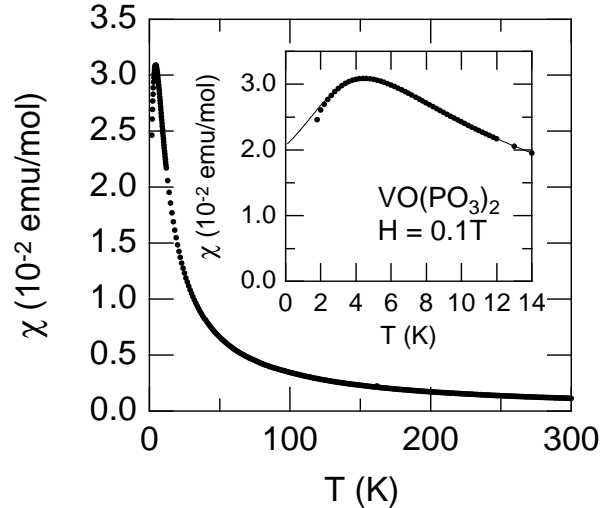


Fig. 2. Temperature dependence of the magnetic susceptibility of α -VO(PO₃)₂. The inner core diamagnetic susceptibility (-9.2×10^{-5} emu/mol) was subtracted from the raw data. The inset is the expanded view at low temperatures. The solid line in the inset is a fit of the data to the susceptibility of an $S = 1/2$ Heisenberg antiferromagnetic linear chain.

can uniquely be determined as the time constant of the recovery curve.

§3. Results and Analysis

3.1 Magnetic Susceptibility

Figure 2 shows the temperature (T) dependence of the bulk magnetic susceptibility (χ) of α -VO(PO₃)₂. While showing Curie-Weiss-like behavior at high temperatures, the susceptibility takes a rounded maximum around $T_{\max} \approx 4.4$ K as a sign of low-dimensional nature of the exchange coupling. The susceptibility can nicely be fitted to the Bonner-Fisher curve for the $S = 1/2$ Heisenberg antiferromagnetic spin chain (HAFC).¹⁸⁾ We estimated the intrachain coupling J between V⁴⁺ spins by fitting the T dependence of the bulk χ to the formula;¹⁹⁾

$$\chi = \chi_0 + \frac{N_A g^2 \mu_B^2}{k_B T} \times \frac{0.25 + 0.14995x + 0.30094x^2}{1 + 1.9862x + 0.68854x^2 + 6.0626x^3}. \quad (3.1)$$

Here χ_0 is a T -independent part of χ , N_A is Avogadro's number, g is Landé's g factor, μ_B is the Bohr magneton and $x = J/k_B T$. From the least-squares fit of all the available data points (1.8 to 300 K), we obtained $\chi_0 = 1.05(8) \times 10^{-5}$ emu/mol, $g = 1.978(1)$ and $J/k_B = 3.50(1)$ K. The result of the fit is shown in the inset of Fig. 2. χ_0 may be interpreted as the Van-Vleck orbital paramagnetic susceptibility χ_{VV} , and the obtained value of χ_0 is in a reasonable range for χ_{VV} of a V⁴⁺ ion. The bulk χ deviates slightly from the Bonner-Fisher curve below about 2.2 K which may be attributed to the effect of the interchain coupling. As expected, a transition to the long-range ordered state is found to occur at 1.93 K.

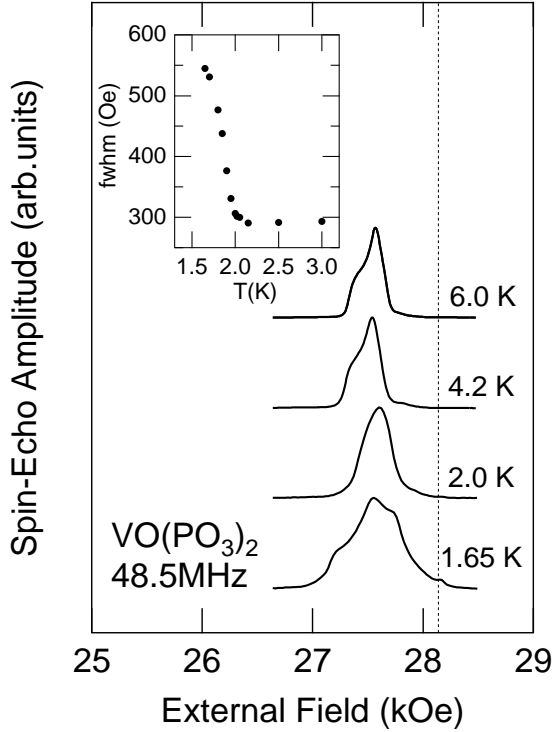


Fig. 3. Temperature variation of the field-swept NMR spectrum of ^{31}P in α -VO(PO₃)₂ taken at 48.5 MHz. The dotted line indicates a zero-shift position for ^{31}P . The inset shows the temperature dependence of FWHM of the spectrum.

3.2 NMR spectrum and the Knight shift

Typical examples of the field-swept ^{31}P NMR spectrum are shown in Fig. 3. Above 2.0 K the spectrum exhibits an asymmetric pattern resulting from an axially-symmetric Knight-shift tensor. The spectrum at 2.0 K has some broadening as manifested by smearing of the fine structure which appears at higher temperatures. As the temperature is decreased further, the line becomes broader and exhibits again a characteristic shape with two shoulders on both sides of the peak (except the small one near the zero shift which probably comes from a trace of nonmagnetic impurity phases). The broadening of the spectrum signals the onset of long-range magnetic ordering of V^{4+} spins giving rise to a finite internal magnetic field at the P site. The ordering is considered to be antiferromagnetic because the spectrum is broadened almost symmetrically about its center-of-gravity position in the paramagnetic state. As shown in the inset of Fig. 3, the FWHM of the spectrum exhibits a sudden increase around 2.0 K which gives a rough estimate of the Néel temperature T_N . Indeed, we determined T_N more precisely from the T dependence of the nuclear spin-lattice relaxation rate $1/T_1$ at the P site to be 1.93(1) K where $1/T_1$ is strongly peaked due to critical slowing down of the electronic spins (see Fig. 5).

The NMR spectrum below T_N does not have a rectangular shape which we usually observe for nonmagnetic nuclei in collinear antiferromagnets. The observed line shape, however, can be explained as the one in

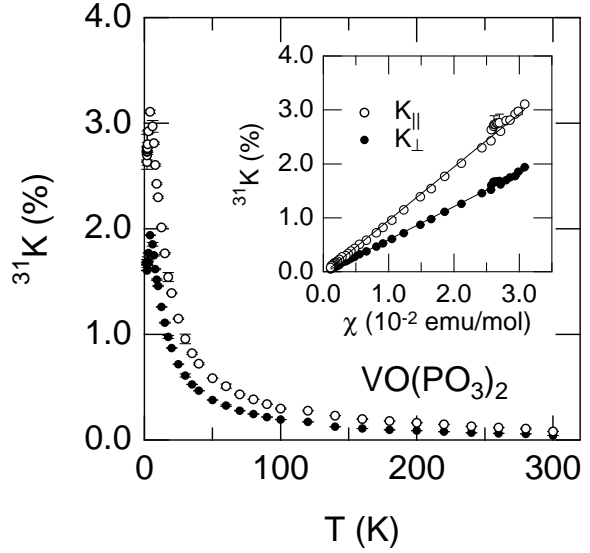


Fig. 4. Temperature dependence of the principal values of the Knight-shift tensor, K_{\parallel} (open circles) and K_{\perp} (solid circles), at the P site in α -VO(PO₃)₂. The inset shows the K - χ plot for each principal component. The solid lines in the inset are the linear fit of the data, the slopes of which yield the hyperfine coupling constants A_{\parallel} and A_{\perp} .

the two-sublattice antiferromagnet by taking account of 1) the anisotropy of the hyperfine coupling resulting in the anisotropic Knight-shift tensor in the paramagnetic state, 2) incomplete cancellation of the transferred hyperfine fields from neighboring V^{4+} spins belonging to different sublattices due to the difference of the interatomic distances between V and P atoms, and 3) small tipping in the moment direction from the easy axis under the applied field of which effect is expressed by the parallel and perpendicular susceptibilities. Details of the calculation and the simulation of the spectrum will be given in the appendix, and we only mention here that as shown in Fig. 11 the observed spectrum is well reproduced using physically-reasonable parameters.

From the values of the intrachain coupling J and the Néel temperature T_N , we can estimate the interchain coupling. The interchain coupling J' may be evaluated using the expression²⁰⁾

$$\frac{T_N}{J} = \sqrt{\frac{z|J'|}{2J}}. \quad (3.2)$$

Substituting $T_N = 1.93$ K and $J/k_B = 3.50$ K into eq. (3.2), we obtain $z|J'|/k_B = 2.13$ K. If we disregard for simplicity the difference between the second and third nearest neighbor V-V distances,²¹⁾ $z = 4$ and we get the “average” interchain coupling $|J'|/k_B = 0.53$ K (the sign cannot be specified). The ratio $|J'|/J = 0.15$ between the intra- and interchain exchange couplings is much larger than those of the other well-known examples of a 1D magnet having J'/J of order 10^{-2} or less.

A careful analysis of the line shape in the paramagnetic state enables us an independent determination of the principal values of the Knight-shift tensor.²²⁾ We plotted

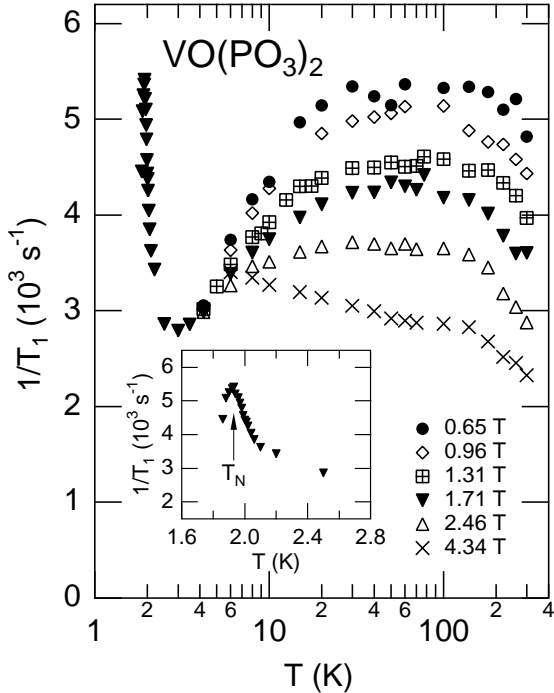


Fig. 5. Temperature dependence of the nuclear spin-lattice relaxation rate at the P site in α -VO(PO₃)₂ measured at various magnetic fields. The inset shows the relaxation rate near T_N measured at 1.71 T.

in Fig. 4 the T dependence of the two independent principal components of the Knight-shift tensor, K_{\parallel} and K_{\perp} , which correspond to the shift for the magnetic-field direction parallel and perpendicular to the symmetry axis at the P site, respectively. The Knight-shift tensor depends strongly on temperature and takes a maximum at 4.2 K as the bulk χ . As shown in the inset of Fig. 4, both K_{\parallel} and K_{\perp} scale with the bulk χ above and below the susceptibility maximum. From the linear slopes of the K_{\parallel} and K_{\perp} versus χ plots, we determined the principal components of the hyperfine tensor at the P site to be $A_{\parallel} = 5.5(1)$ kOe/ μ_B and $A_{\perp} = 3.3(1)$ kOe/ μ_B . These values yield the isotropic and uniaxial components of the hyperfine coupling, $A_{\text{iso}} = (A_{\parallel} + 2A_{\perp})/3 = 4.1(1)$ kOe/ μ_B and $A_{\text{ax}} = (A_{\parallel} - A_{\perp})/3 = 1.1(1)$ kOe/ μ_B , respectively. The hyperfine coupling at the P site is dominated by an isotropic transferred hyperfine field from the neighboring V⁴⁺ spins and has a small anisotropic component. A_{ax} is much larger than is expected from the classical dipolar field of the surrounding V⁴⁺ spins (~ 0.18 kOe/ μ_B) and may be attributed to polarization of anisotropic p orbitals on the P atom.

3.3 Nuclear spin-lattice relaxation

Figure 5 shows the T dependence of the nuclear spin-lattice relaxation rate $1/T_1$ at the P site under various magnetic fields. The relaxation rate is strongly field dependent and is larger at lower fields. The field dependence becomes weaker as the temperature decreases, and $1/T_1$ becomes almost field-independent at 4.2 K. As

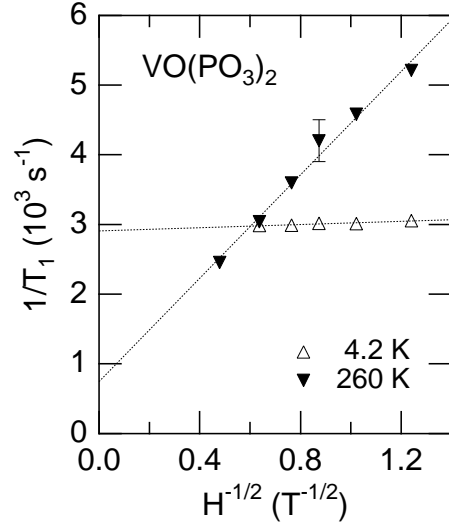


Fig. 6. Nuclear spin-lattice relaxation rate at the P site in α -VO(PO₃)₂ as a function of $H^{-1/2}$ at two different temperatures. The dotted lines are the fit of the data to the formula $1/T_1 = P + QH^{-1/2}$.

to the T dependence, $1/T_1$ measured at different fields have some common characteristics. At high temperatures above about 50 K, $1/T_1$ is only weakly T dependent and decreases gradually on increasing temperature. On the other hand, the relaxation rate decreases rapidly below about 50 K except the rate at the field $H = 4.34$ T showing a modest upturn in that temperature region. Note that the decrease of $1/T_1$ at low temperatures is more pronounced at lower fields. Below about 2.5 K, $1/T_1$ exhibits a critical increase toward the long-range magnetic-ordering temperature as shown in the inset of Fig. 5. The maximum of $1/T_1$ is observed at 1.93 K which we determined as the Néel temperature of this compound.

The strong magnetic-field (H) dependence of $1/T_1$ is likely to come from spin diffusion characteristic of a low-dimensional Heisenberg spin system. In one dimension the spectral density of the spin-spin correlations diverges as $\omega^{-1/2}$ toward $\omega \rightarrow 0$ which can be probed as $H^{-1/2}$ dependence of $1/T_1$. Figure 6 shows examples of the H dependence of $1/T_1$ at the P site plotted as a function of $H^{-1/2}$. It is clear that $1/T_1$ at high temperatures obeys an $H^{-1/2}$ law indicating diffusive behavior of the spin-spin correlations. The field dependence can be fitted to the form

$$1/T_1 = P + QH^{-1/2} \quad (3.3)$$

where P and Q are fitting constants. While the second term represents the contribution of spin diffusion near $q = 0$, the first term includes all possible field-independent contributions to $1/T_1$. We analyzed the measured $1/T_1$ based on eq. (3.3) down to 4.2 K to parametrize the T and H dependence of $1/T_1$, although the phenomenological theory of spin diffusion is justified in the limit $T \gg J/k_B$. Physical meanings of the ob-

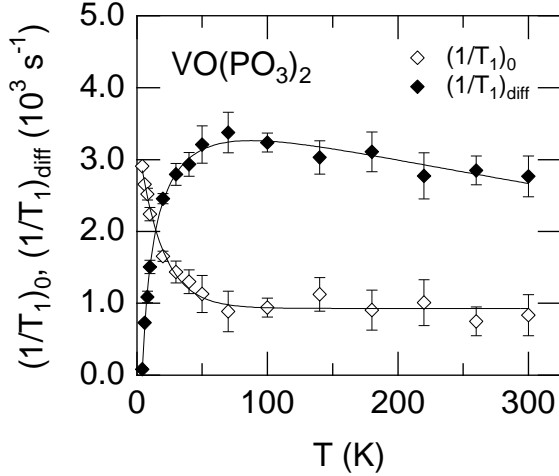


Fig. 7. Temperature dependence of the field-independent relaxation rate $(1/T_1)_0$ (open symbols) and the diffusive contribution $(1/T_1)_{\text{diff}}$ at 1.71 T (solid symbols). The solid lines are guides to the eyes.

tained parameters will be examined in the next section. Returning to Fig. 6, the diffusive contribution proportional to $H^{-1/2}$ dominates the nuclear-spin relaxation at 260 K. The slope in $H^{-1/2}$ decreases monotonically with decreasing temperature while the field-independent part of $1/T_1$ grows up. The $H^{-1/2}$ contribution vanishes almost entirely at 4.2 K, so that $1/T_1$ is governed by field-independent relaxation processes. Takigawa *et al.* reported a weak H dependence of $1/T_1$ in Sr₂CuO₃ with a decreasing slope in the $1/T_1$ vs $H^{-1/2}$ plot on cooling,¹⁴ similar to the behavior of $1/T_1$ at the P site in α -VO(PO₃)₂ at low temperatures.

The T dependence of the field-independent relaxation rate $(1/T_1)_0 \equiv P$ is shown in Fig. 7. $(1/T_1)_0$ is almost T independent with the value of about $1.0 \times 10^3 \text{ s}^{-1}$ above 50 K. Below about 50 K, on the other hand, a substantial increase of $(1/T_1)_0$ was observed. This is contrasted with the behavior of $1/T_1$ in that temperature region where $1/T_1$ decreases rapidly on cooling. The low- T decrease of $1/T_1$ therefore results from the decrease of diffusive contribution which overrides the increasing contribution of $(1/T_1)_0$. It is likely that the increase of $(1/T_1)_0$ from the high- T asymptotic value is caused by an enhancement of short-range AF correlations within the chain, because geometry at the P site allows intrachain AF spin fluctuations to contribute to the ³¹P nuclear-spin relaxation.

In Fig. 7 we also show for comparison the T dependence of diffusive contribution $(1/T_1)_{\text{diff}} = 1/T_1 - (1/T_1)_0$ at 1.71 T. It is clear that, while governing $1/T_1$ at higher temperatures, $(1/T_1)_{\text{diff}}$ decreases rapidly below about 50 K. The decrease of $(1/T_1)_{\text{diff}}$ synchronizes with the increase of $(1/T_1)_0$, which strongly suggests some common origin for them. As mentioned above, the intrachain short-range AF correlation is a likely source for such T -dependent behavior of the nuclear-spin relaxation.

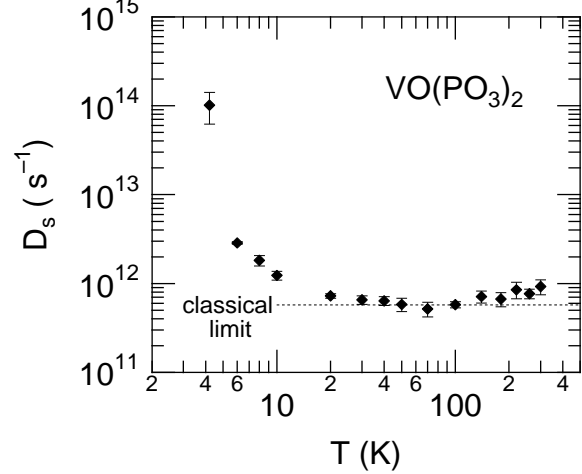


Fig. 8. Temperature dependence of the spin-diffusion constant D_s . The dotted line is a value of D_s in the classical limit.

From the slope Q of the $1/T_1$ versus $H^{-1/2}$ plot, we can estimate the spin-diffusion constant D_s which determines the decay of the spin-spin correlation functions for small q as $\langle S_q^x(t)S_{-q}^x(0) \rangle \propto \exp(-D_s q^2 t) \exp(-i\omega_e t)$ where $\omega_e = g\mu_B H/\hbar$ is the electron Larmor frequency.²⁴ If the hyperfine coupling is predominantly isotropic which is the case for the P site in α -VO(PO₃)₂, the transverse component of the spectral density $S_{xx}(\omega) = \Sigma_q \int_{-\infty}^{\infty} dt e^{i\omega t} \{S_q^x(t), S_{-q}^x(0)\}$ dominates the H -dependent part of $1/T_1$. The nuclear spin-lattice relaxation rate $(1/T_1)_{\text{diff}}$ due to spin diffusion is then given as

$$\left(\frac{1}{T_1}\right)_{\text{diff}} = \frac{A^2 k_B T}{\hbar^2 g^2 \mu_B^2} \frac{\chi_{\text{spin}}}{\sqrt{2D_s \omega_e}} \quad (3.4)$$

in one dimension. Here A is the hyperfine coupling constant in units of energy and χ_{spin} is the spin susceptibility per magnetic atom. We determined D_s using the values A_{iso} for A , $\chi_{\text{spin}} = (\chi - \chi_0)/N_A$ and g determined from the analysis of the susceptibility and the Knight shift. The result is shown in Fig. 8 where D_s is plotted as a function of temperature. D_s is nearly T independent with the value of $(6 - 8) \times 10^{11} \text{ s}^{-1}$ above 20 K. It agrees well with the classical limit⁸) $(J/\hbar)\sqrt{2\pi S(S+1)/3} = 5.7 \times 10^{11} \text{ s}^{-1}$, which suggests that the spin dynamics is governed by the classical spin diffusion. On the other hand, D_s becomes unusually large below about 10 K compared with the classical value. Such an anomalously large D_s may be a signature that spin diffusion no longer describes the intrinsic dynamics of the $S = 1/2$ HAFC at low temperatures.

§4. Discussion

Although α -VO(PO₃)₂ undergoes a long-range AF transition at $T_N = 1.93$ K, the spin dynamics still possesses a one-dimensional (1D) diffusive character at high temperatures as manifested by the strong $H^{-1/2}$ dependence of $1/T_1$. On the one hand, a weaker field dependence of $1/T_1$ below about 50 K implies low-energy spin

excitations being governed by different physics at lower temperatures. The change of the H -dependent behavior of $1/T_1$ around 50 K is nothing but an evidence for crossover between the two distinct temperature regimes of interest we mentioned in the Introduction, the paramagnetic regime $T \gg J/k_B$ at temperatures well above the intrachain exchange and the short-range-ordered (SRO) regime $T \sim J/k_B$ with strong intrachain AF correlations.

In the paramagnetic regime above about 50 K, physical quantities characterizing the dynamics such as $1/T_1$, $(1/T_1)_0$ and D_s are nearly T independent. $1/T_1$ is governed by 1D diffusive spin excitation near $q = 0$ giving rise to the $H^{-1/2}$ dependence of $1/T_1$ at the P site. On the other hand, the field-independent relaxation rate $(1/T_1)_0$ remains small. The spin-diffusion constant D_s in this temperature regime is in good agreement with the value expected in the classical limit, which suggests that the observed diffusive behavior is an intrinsic property of the spin system but not an effect of the coupling with the other degrees of freedom such as phonons.³⁾

It has been argued that the field-independent relaxation rate in the paramagnetic diffusion regime comes from the longitudinal component of the spectral density $S_{zz}(\omega)$, of which divergence toward $\omega \rightarrow 0$ is cutoff by interactions that break the conservation of the intrachain uniform magnetization.^{8,9)} Here we estimate such a contribution to $(1/T_1)_0$. The cutoff effect is taken into account phenomenologically by multiplying the exponential decay to the longitudinal diffusive spin correlation function as $\langle S_q^z(t)S_{-q}^z(0) \rangle \propto \exp(-D_s q^2 t) \exp(-\omega_c t)$ where ω_c is the cutoff frequency.^{12,13)} On the assumption that the nuclear Larmor frequency is much smaller than ω_c , the relaxation rate $(1/T_1)_{\text{cutoff}}$ due to the longitudinal component with cutoff is given as

$$\left(\frac{1}{T_1}\right)_{\text{cutoff}} = \frac{A'^2 k_B T}{\hbar^2 g^2 \mu_B^2} \frac{\chi_{\text{spin}}}{\sqrt{D_s \omega_c}} \quad (4.1a)$$

which in the limit $T \rightarrow \infty$ can be written as

$$\left(\frac{1}{T_1}\right)_{\text{cutoff}} = \frac{A'^2 S(S+1)}{\hbar^2 3\sqrt{D_s \omega_c}}. \quad (4.1b)$$

Here A' is the relevant coupling constant which in the present case is of dipolar origin. An important cutoff mechanism in α -VO(PO₃)₂ is the interchain coupling much larger than the dipolar coupling between electronic spins. Taking $\omega_c = k_B J'/\hbar \approx 7 \times 10^{10} \text{ s}^{-1}$ and $D_s \approx 7 \times 10^{11} \text{ s}^{-1}$, and using the dipolar coupling constant ($\sim 0.18 \text{ kOe}/\mu_B$) for A' , we obtain $(1/T_1)_{\text{cutoff}} = 17 \text{ s}^{-1}$ from eq. (4.1b). This is nearly two orders-of-magnitude smaller than the observed $(1/T_1)_0$. Even if we take smaller ω_c due to the electron dipolar coupling ($\sim 0.05 \text{ K}$), $(1/T_1)_{\text{cutoff}}$ is at most 54 s^{-1} and cannot explain the observed $(1/T_1)_0$. The above estimate of $(1/T_1)_{\text{cutoff}}$ leads us to conclude that the field-independent relaxation rate $(1/T_1)_0$ in the paramagnetic regime is determined by the mechanism other than spin diffusion, although the origin is not clear at present. It is noted that the exchange-narrowing limit of $1/T_1$ ²³⁾ calculated using parameters for α -VO(PO₃)₂ as $1/T_{1\infty} = 2.6 \times 10^3 \text{ s}^{-1}$ cannot explain as well the value of $(1/T_1)_0$ at high

temperatures.

Next we discuss the dynamics at low temperatures below about 50 K. An important observation in this SRO regime is a decreasing contribution of spin diffusion to $1/T_1$. Concurrently with a growth of intrachain AF correlations, diffusive excitations become less important as a possible channel for nuclear-spin relaxation, and at temperatures $T \approx J/k_B$ where the AF alignment of the spins along the chain is almost established, the diffusive contribution becomes essentially absent. This accompanies an increase of D_s as a fitting variable from the T -independent asymptotic value in the paramagnetic regime. The apparent increase of D_s , however, seems to make no quantitative sense because D_s is estimated using eq. (3.4) which is justified in the limit $T \gg J/k_B$. It may rather suggest the classical spin-diffusion theory becoming inapplicable in the SRO regime: D_s cannot be defined as a physical-meaningful spin-diffusion constant. This may result from a qualitative change of the intrinsic dynamics of the $S = 1/2$ HAFC from diffusive to nondiffusive, possibly propagating ones as approaching $T \approx J/k_B$.

It should be noted that the breakdown of the classical spin-diffusion theory due to SRO does not affect the qualitative behavior of $(1/T_1)_0$. Since $1/T_1$ tends to be H -independent as the temperature decreases, it is expected that the result for $(1/T_1)_0$ does not depend on the precise form of $1/T_1$ as a function of H . We may therefore conclude that the low- T increase of $(1/T_1)_0$ is not an artifact but an intrinsic property of the system. Although we cannot exclude a possibility that the unidentified H -independent contribution in the paramagnetic regime dominates $(1/T_1)_0$ in the SRO regime as well, it seems reasonable to consider that the increase of $(1/T_1)_0$ comes from a growing contribution of the AF excitation mode because $1/T_1$ exhibits a divergent behavior toward T_N .

In summary, the low-frequency spin dynamics in α -VO(PO₃)₂ is characterized by the two distinct temperature regimes and the crossover behavior between them. In the high- T regime ($T \gg J/k_B$) $1/T_1$ is dominated by the H -dependent diffusive contribution which is described quantitatively by the 1D classical spin-diffusion theory. As the temperature approaches the intrachain coupling strength J/k_B , the system goes into a different regime with an almost H -independent $1/T_1$. If we continue to analyze $1/T_1$ in terms of the classical spin-diffusion theory, we observe an apparent increase of the spin-diffusion constant from the classical limit. It represents parametrically the decrease of diffusive contribution to $1/T_1$, and may be interpreted as a sign of crossover to the low- T regime with nondiffusive, propagating spin excitations.

Appendix: Analysis of the NMR Line Shape in the Antiferromagnetic State

The NMR line shape observed in the antiferromagnetic (AF) state is unusual and is to be examined further. We present in this appendix the derivation of the resonance condition appropriate for this specific example and may be applicable if the hyperfine coupling at

the nuclear site under consideration has uniaxial symmetry. We also give the calculation of the line shape using the derived resonance condition. From comparison of the calculated spectrum with the observed one, it is shown that the observed line shape below T_N is in consistency with collinear antiferromagnetic structure having two sublattices. The point of derivation is to take account of an anisotropy of the hyperfine coupling, incomplete cancellation of the transferred hyperfine fields from neighboring magnetic ions, and field-induced canting of sublattice magnetizations.

The resonance frequency ω for nuclei with the nuclear gyromagnetic ratio γ is generally given as

$$\omega/\gamma = |\mathbf{H}_0 + \mathbf{H}_n|. \quad (\text{A}\cdot 1)$$

Here \mathbf{H}_0 and \mathbf{H}_n are external and internal magnetic fields, respectively. Neglecting the classical dipolar field for the time being, \mathbf{H}_n is due to the hyperfine field and is given as

$$\mathbf{H}_n = \sum_j \tilde{\mathbf{A}}_{ij} \cdot \mathbf{S}_j \quad (\text{A}\cdot 2)$$

where \mathbf{S}_j is the electronic spin at the j -th site and $\tilde{\mathbf{A}}_{ij}$ is the hyperfine tensor between the sites i and j . \mathbf{S}_j fluctuates in time and hence \mathbf{H}_n in eq. (A·1) should be the time average because we are dealing with the resonance frequency. For simplicity of notation we omit the brackets $\langle \rangle$ to show explicitly the time-averaging procedure and use \mathbf{S}_j and \mathbf{H}_n as the time-averaged quantities in the following.

In α -VO(PO₃)₂, there are two neighboring V atoms in the distances 3.292 Å and 3.392 Å around the P site and the others are relatively far apart (≥ 4.613 Å). Because a transferred hyperfine coupling is generally short-ranged, we may consider a contribution of these two V atoms to \mathbf{H}_n at the P site. Labelling these V sites as V(1) and V(2), and similarly the electronic spins as \mathbf{S}_1 and \mathbf{S}_2 , we can rewrite eq. (A·2) as

$$\mathbf{H}_n = \tilde{\mathbf{A}}_1 \cdot \mathbf{S}_1 + \tilde{\mathbf{A}}_2 \cdot \mathbf{S}_2 \quad (\text{A}\cdot 3)$$

for the P site in α -VO(PO₃)₂. Here $\tilde{\mathbf{A}}_1$ and $\tilde{\mathbf{A}}_2$ are the hyperfine tensors from V(1) and V(2) sites, respectively. Since V(1) and V(2) belong to the different AF chains, \mathbf{S}_1 and \mathbf{S}_2 can in principle be either parallel or antiparallel in zero external field.

If \mathbf{S}_1 and \mathbf{S}_2 are parallel, i.e., V(1) and V(2) belong to the same sublattice, $\mathbf{S}_1 = \mathbf{S}_2$ and hence $\mathbf{H}_n = (\tilde{\mathbf{A}}_1 + \tilde{\mathbf{A}}_2) \cdot \mathbf{S}_1$. Because the sum $\tilde{\mathbf{A}}_1 + \tilde{\mathbf{A}}_2$ corresponds to the hyperfine tensor in the paramagnetic state, there should be a transferred field of significant magnitude (a few kOe) at the P site. We expect in that case a usual rectangular shape of the spectrum which contradicts with the observation. We therefore assume antiparallel alignment of \mathbf{S}_1 and \mathbf{S}_2 under zero external field which means that V(1) and V(2) belong to different sublattices.

Under nonzero external field, the sublattice moment changes its direction and magnitude slightly from the zero-field values. If the external field is smaller than the spin-flop field, the effect may be expressed by the parallel

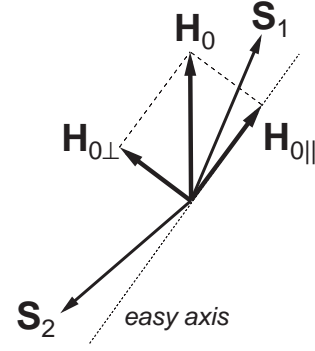


Fig. 9. Schematic view of the canting due to the external field \mathbf{H}_0 of the electronic spins \mathbf{S}_1 and \mathbf{S}_2 . The dotted line indicates the direction of the easy axis. Decomposition of \mathbf{H}_0 to the components parallel and perpendicular to the easy axis, $\mathbf{H}_{0||}$ and $\mathbf{H}_{0\perp}$, respectively, is also shown.

and perpendicular susceptibilities, $\chi_{||}$ and χ_{\perp} , in the AF state. It is then convenient to decompose \mathbf{S}_1 and \mathbf{S}_2 into components parallel and perpendicular to the easy axis for the sublattice moment as $\mathbf{S}_j = \mathbf{S}_{j||} + \mathbf{S}_{j\perp}$ ($j = 1, 2$) and similarly the external field as $\mathbf{H}_0 = \mathbf{H}_{0||} + \mathbf{H}_{0\perp}$ (Fig. 9). The following relations hold between the susceptibilities and the parallel and perpendicular components of \mathbf{S}_1 , \mathbf{S}_2 and \mathbf{H}_0 ;

$$\mathbf{S}_{1||} + \mathbf{S}_{2||} = 2\chi_{||}\mathbf{H}_{0||}, \quad (\text{A}\cdot 4\text{a})$$

$$\mathbf{S}_{1\perp} + \mathbf{S}_{2\perp} = 2\chi_{\perp}\mathbf{H}_{0\perp}. \quad (\text{A}\cdot 4\text{b})$$

Here $\chi_{||}$ and χ_{\perp} are defined as the susceptibilities per magnetic atom. Defining $\tilde{\mathbf{A}} = \tilde{\mathbf{A}}_1 + \tilde{\mathbf{A}}_2$ and $\tilde{\mathbf{a}} = \tilde{\mathbf{A}}_1 - \tilde{\mathbf{A}}_2$, eq. (A·3) can be written as

$$\begin{aligned} \mathbf{H}_n &= \chi_{\perp}\tilde{\mathbf{A}} \cdot \mathbf{H}_{0\perp} + \chi_{||}\tilde{\mathbf{A}} \cdot \mathbf{H}_{0||} \\ &+ \frac{1}{2}[\tilde{\mathbf{a}} \cdot (\mathbf{S}_{1\perp} - \mathbf{S}_{2\perp}) + \tilde{\mathbf{a}} \cdot (\mathbf{S}_{1||} - \mathbf{S}_{2||})] \end{aligned} \quad (\text{A}\cdot 5)$$

$$\approx \chi_{\perp}\tilde{\mathbf{A}} \cdot \mathbf{H}_{0\perp} + \chi_{||}\tilde{\mathbf{A}} \cdot \mathbf{H}_{0||} + \tilde{\mathbf{a}} \cdot \mathbf{S}_{1||}. \quad (\text{A}\cdot 6)$$

On going from (A·5) to (A·6) we used the approximations $\mathbf{S}_{1||} \approx -\mathbf{S}_{2||}$ and $\mathbf{S}_{1\perp} \approx \mathbf{S}_{2\perp}$. The first and second terms in eq. (A·6) correspond to the hyperfine field resulting from canting of \mathbf{S}_1 and \mathbf{S}_2 from the easy axis under nonzero external field. The third term represents the hyperfine field due to the difference between $\tilde{\mathbf{A}}_1$ and $\tilde{\mathbf{A}}_2$. Putting $\tilde{\mathbf{a}} \cdot \mathbf{S}_{1||} = \mathbf{H}_{n0}$ in eq. (A·6) gives a more convenient form for \mathbf{H}_n ;

$$\mathbf{H}_n = \chi_{\perp}\tilde{\mathbf{A}} \cdot \mathbf{H}_{0\perp} + \chi_{||}\tilde{\mathbf{A}} \cdot \mathbf{H}_{0||} + \mathbf{H}_{n0}. \quad (\text{A}\cdot 7)$$

As has been pointed out, \mathbf{H}_{n0} comes from uncancellation of the hyperfine fields from the two neighboring V atoms.

In deriving the expression of the resonance condition from which the line shape is calculated, we have to take some orthogonal frame and specify the directions of \mathbf{H}_0 and \mathbf{H}_{n0} . It is reasonable to take the principal frame of the hyperfine tensor $\tilde{\mathbf{A}}$ at the P site in which $\tilde{\mathbf{A}}$ is diagonalized and the principal values are known from the experiment. Taking the z axis as the unique axis of the tensor $\tilde{\mathbf{A}}$ having axial symmetry, we denote the

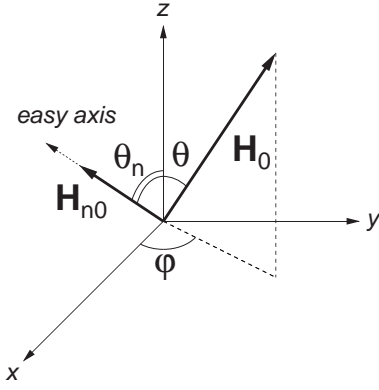


Fig. 10. Principal frame used in the calculation of the resonance frequency. The dotted line with an arrow indicates the direction of the easy axis. The easy axis is taken to be in the xz plane.

directions of the easy axis and the external field \mathbf{H}_0 by the polar and azimuth angles as shown in Fig. 10. The easy axis can be taken to lie in the xz plane so that $\varphi_n = 0$ without loss of generality because of the axial symmetry of $\tilde{\mathbf{A}}$. For the field \mathbf{H}_{n0} we assume that it is in the direction of the easy axis for simplicity. This is equivalent to neglect the anisotropy of $\tilde{\mathbf{a}}$. It is noted that with this assumption, the classical dipolar field may be included in \mathbf{H}_{n0} so that \mathbf{H}_{n0} is regarded as the sum of classical dipolar and hyperfine fields, because the dipolar field is a likely source for the anisotropy field in the $S = 1/2$ system and may be taken to be parallel to the easy axis.

Our aim is to express the resonance frequency ω as a function of the angles θ , φ and θ_n , and the field strength $H_0 = |\mathbf{H}_0|$ and $H_{n0} = |\mathbf{H}_{n0}|$. The angles θ and φ distribute randomly in the polycrystalline sample, so that a specific line shape called powder pattern is observed. In the principal frame of $\tilde{\mathbf{A}}$, \mathbf{H}_0 and \mathbf{H}_n are written explicitly as follows;

$$\tilde{\mathbf{A}} = \begin{pmatrix} A_x & & \\ & A_y & \\ & & A_z \end{pmatrix} = \begin{pmatrix} A_{\perp} & & \\ & A_{\perp} & \\ & & A_{\parallel} \end{pmatrix}, \quad (\text{A}\cdot 8\text{a})$$

$$\mathbf{H}_0 = \begin{pmatrix} b_x H_0 \\ b_y H_0 \\ b_z H_0 \end{pmatrix} = \begin{pmatrix} H_0 \sin \theta \cos \varphi \\ H_0 \sin \theta \sin \varphi \\ H_0 \cos \theta \end{pmatrix}, \quad (\text{A}\cdot 8\text{b})$$

$$\mathbf{H}_{n0} = \begin{pmatrix} c_x H_{n0} \\ 0 \\ c_z H_{n0} \end{pmatrix} = \begin{pmatrix} H_{n0} \sin \theta_n \\ 0 \\ H_{n0} \cos \theta_n \end{pmatrix}. \quad (\text{A}\cdot 8\text{c})$$

A_{\parallel} and A_{\perp} are the principal values of $\tilde{\mathbf{A}}$ which can be determined from the K - χ plots in the paramagnetic state. $\mathbf{H}_{0\parallel}$ is just the projection of \mathbf{H}_0 onto \mathbf{H}_{n0} , and hence $\mathbf{H}_{0\parallel}$ and $\mathbf{H}_{0\perp}$ can also be written down by components. Substituting eq. (A.7) into eq. (A.1) and writing explicitly the components in the principal frame of $\tilde{\mathbf{A}}$ using eqs. (A.8), we get after lengthy calculations

$$\omega^2 = \omega_x^2 + \omega_y^2 + \omega_z^2 \quad (\text{A}\cdot 9\text{a})$$

with

$$\begin{aligned} \omega_x/\gamma &= [\{1 + A_{\perp}(c_x^2 \chi_{\parallel} + c_z^2 \chi_{\perp})\}b_x \\ &\quad + A_{\perp}(\chi_{\parallel} - \chi_{\perp})c_x c_z b_z]H_0 + c_x H_{n0}, \\ \omega_y/\gamma &= (1 + A_{\perp} \chi_{\perp})b_y H_0, \\ \omega_z/\gamma &= [\{1 + A_{\perp}(c_z^2 \chi_{\parallel} + c_x^2 \chi_{\perp})\}b_z \\ &\quad + A_{\parallel}(\chi_{\parallel} - \chi_{\perp})c_x c_z b_x]H_0 + c_z H_{n0}. \end{aligned} \quad (\text{A}\cdot 9\text{b})$$

Note that χ_{\parallel} (χ_{\perp}) is not the susceptibility for the z (x, y) direction(s) in the principal frame of $\tilde{\mathbf{A}}$ but the one parallel (perpendicular) to the easy axis. Neglecting the terms of $O(A^2 \chi^2)$, and using the relations $b_x^2 + b_y^2 + b_z^2 = 1$ and $c_x^2 + c_z^2 = 1$, eq. (A.9) can be rewritten as

$$\begin{aligned} \omega^2/\gamma^2 &= H_0^2 + H_{n0}^2 + 2(b_x c_x + b_z c_z)H_0 H_{n0} \\ &\quad + 2[A_{\perp}(c_x^2 \chi_{\parallel} + c_z^2 \chi_{\perp})b_x^2 + A_{\perp} \chi_{\perp} b_y^2 \\ &\quad + A_{\parallel}(c_z^2 \chi_{\parallel} + c_x^2 \chi_{\perp})b_z^2 \\ &\quad + (A_{\parallel} + A_{\perp})(\chi_{\parallel} - \chi_{\perp})b_x b_z c_x c_z]H_0^2 \\ &\quad + 2[A_{\perp}(c_x^2 \chi_{\parallel} + c_z^2 \chi_{\perp})b_x c_x \\ &\quad + A_{\parallel}(c_z^2 \chi_{\parallel} + c_x^2 \chi_{\perp})b_z c_z \\ &\quad + A_{\parallel}(\chi_{\parallel} - \chi_{\perp})c_z^2 b_x c_x \\ &\quad + A_{\perp}(\chi_{\parallel} - \chi_{\perp})c_x^2 b_z c_z]H_0 H_{n0}. \end{aligned} \quad (\text{A}\cdot 10)$$

Equation (A.10) is valid for arbitrary strength of H_{n0} as far as the conditions $A\chi \ll 1$ are satisfied.

If H_{n0} is much larger than $A\chi$, eq. (A.10) may be simplified as

$$\omega^2/\gamma^2 = H_0^2 + H_{n0}^2 + 2(b_x c_x + b_z c_z)H_0 H_{n0} \quad (\text{A}\cdot 11\text{a})$$

which, by denoting the angle between \mathbf{H}_0 and \mathbf{H}_{n0} as β , reduces to

$$\omega^2/\gamma^2 = H_0^2 + H_{n0}^2 + 2H_0 H_{n0} \cos \beta. \quad (\text{A}\cdot 11\text{b})$$

Random distribution of β in the polycrystalline sample yields a usual rectangular shape of the spectrum.²⁵⁾

If H_{n0} is much smaller than H_0 but is comparable with $A\chi$ which is the case here, we may neglect in eq. (A.10) the terms proportional to H_{n0}^2 or $A\chi H_{n0}$. Hence we arrive at the final expression of the resonance frequency;

$$\begin{aligned} \omega/\gamma &= H_0 + [A_{\perp}(c_x^2 \chi_{\parallel} + c_z^2 \chi_{\perp})b_x^2 + A_{\perp} \chi_{\perp} b_y^2 \\ &\quad + A_{\parallel}(c_z^2 \chi_{\parallel} + c_x^2 \chi_{\perp})b_z^2 \\ &\quad + (A_{\parallel} + A_{\perp})(\chi_{\parallel} - \chi_{\perp})b_x b_z c_x c_z]H_0 \\ &\quad + (b_x c_x + b_z c_z)H_{n0}, \end{aligned} \quad (\text{A}\cdot 12)$$

or writing explicitly the dependence on the angles as

$$\begin{aligned} \omega/\gamma &= H_0 + [A_{\perp}(\chi_{\parallel} \sin^2 \theta_n + \chi_{\perp} \cos^2 \theta_n) \sin^2 \theta \cos^2 \varphi \\ &\quad + A_{\perp} \chi_{\perp} \sin^2 \theta \sin^2 \varphi \\ &\quad + A_{\parallel}(\chi_{\parallel} \cos^2 \theta_n + \chi_{\perp} \sin^2 \theta_n) \cos^2 \theta \\ &\quad + \frac{1}{4}(A_{\parallel} + A_{\perp})(\chi_{\parallel} - \chi_{\perp}) \sin 2\theta_n \sin 2\theta \cos \varphi]H_0 \\ &\quad + (\sin \theta_n \sin \theta \cos \varphi + \cos \theta_n \cos \theta)H_{n0}. \end{aligned} \quad (\text{A}\cdot 13)$$

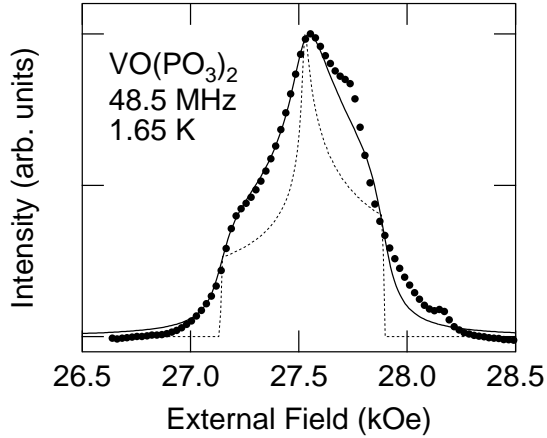


Fig. 11. Comparison of the calculated powder patterns with the observed spectrum at 1.65 K. The solid circles represent the experimental data. The dashed line is the calculated spectrum $f(H_0)$ with no inhomogeneous broadening. The parameters used in the calculation are $\omega = 48.5$ MHz, $A_{\parallel} = 5.5$ kOe/ μ_B , $A_{\perp} = 3.3$ kOe/ μ_B , $H_{n0} = 310$ Oe, $\theta_n = 33^\circ$, $\chi_{\parallel} = 0.026$ emu/mol and $\chi_{\perp} = 0.031$ emu/mol. The spectrum shown by the solid line is calculated by taking account of inhomogeneous distribution of the internal field H_{n0} . The effect is introduced by convoluting lorentzian with the FWHM of 55 Oe.

For the field-sweep measurement the resonance frequency ω is fixed while the external field H_0 is varied. It is therefore necessary to solve eq. (A.13) with respect to H_0 , the result of which is not given here explicitly because it is rather straightforward. Then we calculate the spectrum $f(H_0) \propto \Delta N / \Delta H_0$ by counting the number of nuclei ΔN having the resonance field between H_0 and $H_0 + \Delta H_0$. More than million different (θ, φ) points representing the random distribution of H_0 were taken to calculate the resonance field. The unknowns H_{n0} , θ_n , χ_{\parallel} and χ_{\perp} in (A.13) are treated as parameters to reproduce the observed spectrum. As shown in Fig. 11, an appropriate choice of the parameter values reproduces the observed two-shoulder structure of the spectrum in the AF state. We may therefore conclude that the magnetic ordering in α -VO(PO₃)₂ is not unusual but is rather conventional.

mura: Phys. Rev. Lett. **76** (1996) 2173.

- [13] J. Kikuchi, T. Yamauchi and Y. Ueda: J. Phys. Soc. Jpn. **66** (1997) 1622.
- [14] M. Takigawa, N. Motoyama, H. Eisaki and S. Uchida: Phys. Rev. Lett **76** (1996) 4612.
- [15] E. B. Murashova: Kristallografiya KRISA **39** (1994) 145.
- [16] N. Motoyama, H. Eisaki and S. Uchida: Phys. Rev. Lett. **76** (1994) 3212.
- [17] J. Kikuchi, K. Motoya, T. Yamauchi and Y. Ueda: Phys. Rev. B **60** (1999) 6731.
- [18] J. C. Bonner and M. E. Fisher: Phys. Rev. **135** (1064) A640.
- [19] W. E. Hatfield: J. Appl. Phys. **52** (1981) 1985.
- [20] J. Kondo: Physica B **123** (1984) 169.
- [21] The second and third nearest neighbor V atoms are in the distances of 5.223 Å and 6.092 Å at room temperature.
- [22] A. Abragam: *Principles of Nuclear Magnetism* (Oxford University Press, Oxford, 1961).
- [23] T. Moriya: Prog. Theor. Phys. **16** (1954) 641.
- [24] The power law decay of the spin autocorrelation function $\langle S_i^x(t) S_i^x(0) \rangle \propto t^{-1/2}$ (eq. (1.1)) can be derived by integrating $\langle S_q^x(t) S_{-q}^x(0) \rangle$ over q in one dimensional space.
- [25] J. Kikuchi, K. Ishiguchi, K. Motoya, M. Itoh, K. Inari, N. Eguchi and J. Akimitsu: J. Phys. Soc. Jpn. **69** (2000) 2660.
- [26] S_j fluctuates in time and hence H_n in eq. (A.1) should be the time average because we are dealing with the resonance frequency. For simplicity of notation we omit the brackets $\langle \rangle$ to show explicitly the time-averaging procedure and use S_j and H_n as the time-averaged quantities.

-
- [1] P. G. de Gennes: *Magnetism*, ed. G. T. Rado and H. Suhl (Academic Press, New York, 1963) Vol. III, p. 115.
 - [2] S. Sachdev: Phys. Rev. B **50** (1994) 13006.
 - [3] B. N. Narozhny: Phys. Rev. B **54** (1996) 3311.
 - [4] K. Fabricius and B. M. McCoy: Phys. Rev. B **57**(1998) 8430.
 - [5] F. Naef and X. Zotos: J. Phys. Condens. Matter **10** (1998) L183.
 - [6] B. N. Narozhny, A. J. Millis and N. Andrei: Phys. Rev. B **58** (1998) R2921.
 - [7] X. Zotos: Phys. Rev. Lett. **82** (1999) 1764.
 - [8] D. Hone, C. Scherer and F. Borsa: Phys. Rev. B **9** (1974) 965.
 - [9] F. Borsa and M. Mali: Phys. Rev. B **9** (1974) 2215.
 - [10] Y. Barjhoux, J.-P. Boucher and J. Karra: Physica **86-88** B (1977) 1307.
 - [11] Y. Ajiro, Y. Nakajima, Y. Furukawa and H. Kiriya: J. Phys. Soc. Jpn. **44** (1978) 420.
 - [12] M. Takigawa, T. Asano, Y. Ajiro, M. Mekata and Y. J. Ue-